THE PENNSYLVANIA STATE UNIVERSITY
SCHREYER HONORS COLLEGE

DEPARTMENT OF ASTRONOMY & ASTROPHYSICS

CHARACTERIZING AN EARLY-WARNING SEARCH FOR BINARY NEUTRON STARS IN THE PRESENCE OF NON-STATIONARY NOISE

COLLIN HECKMAN
SPRING 2021

A thesis
submitted in partial fulfillment
of the requirements
for baccalaureate degrees
in Astronomy & Astrophysics and Physics
with honors in Astronomy & Astrophysics

Reviewed and approved* by the following:

Dr. Chad Hanna
Associate Professor of Phsyics & Astronomy and Astrophysics
Thesis Supervisor

Dr. Niel Brandt
Professor of Astronomy and Astrophysics
Honors Adviser

*Electronic Approvals are on file in the Schreyer Honors College.

Abstract

The merging of binary neutron stars (BNSs) produces gravitational waves capable of being detected by Advanced LIGO and Virgo before the time of merger. Therefore, the merger event can be detected before the electromagnetic counterpart. The early warning gravitational wave detection pipeline was previously tested in Sachdev et al. [1]. Here we will build off that testing with an updated method of data recoloring to more closely simulate real signals. We will be narrowing the range of frequencies investigated in the original paper to look solely at 49 Hz. By enabling the early warning of gravitational wave event, an organized observing group including several telescopes has the potential to observe the merger seconds before the event occurs.

Table of Contents

List of Figures

List of Tables

Acknowledgements

I would like to thank my Thesis Supervisor Dr. Chad Hanna and the rest of the Penn State Institute for Gravitation and the Cosmos. In particular I would like to thank Dr. Surabhi Sachdev, Dr. Debnandini Mukherjee, and Dr. Patrick Godwin for their guidance and assistance in my research pursuits. I would also like to thank the Millennium Scholars program for their mentorship and academic support. In particular I would like to thank my Millennium Scholars program coordinator Georjanne Rosa for her assistance.

Lastly, I would like to thank my parents and brothers. Without you I would never have made it this far.

Chapter 1

Introduction to LIGO and Gravitational Wave Detection

1.1 What is a Gravitational Wave?

The first detection of a gravitational wave in 2015 by the Laser Interferometer Gravitational Observatory (LIGO) opened the door for an amazing advancement in astronomy [2]. From this first detection to a mere six years later, LIGO and Virgo have made countless other detections, rapidly expanding what is known about this once purely theoretical topic. Gravitational waves offer the potential to expand astronomy and physic's scope of knowledge. They are both a wonder themselves as well as a gateway into new observations of previously hard to observe objects.

Gravitational waves as explained by Einstein are a wave of spatial strain [2]. That description can be rephrased to say that they are ripple that travels through spacetime distorting space as they pass through. This distortion appears as a form of compression or expansion changing the distance between objects as the waves pass through as is visible in Figure 11.1. The magnitude of these distortions vary along with the frequency at which a wave passes through meaning that an observation of these parameters reveals information about the source of the wave.

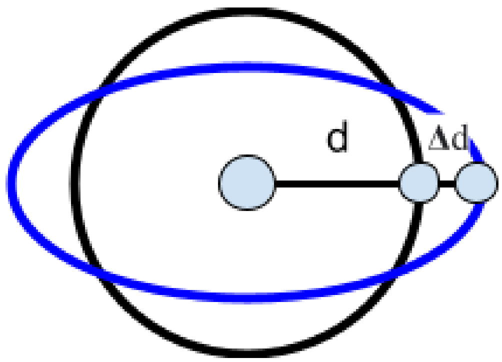

Figure 1.1: Strain causes a distortion in distances. In this example the strain causes a difference in distance between the center sphere and the side sphere of Δd.

The first prediction of gravitational waves was done by Einstein as part of his Theory of General Relativity back in 1916 [2]. In Einstein's work he predicted a wave of spatial strain. In this case strain is a dimensionless quantity defined as h, that gives the fractional change in length of space [3]. Additionally strain is the amplitude of the gravitational wave. Evolving from Einstein's original work, the energy loss by systems such as that of a binary system of two non-spinning compact objects which is given by

$$\frac{dE}{dt} \simeq \frac{32G}{5c^5}\eta^5(\frac{Gm}{rc^2})^5 \tag{1.1}$$

where $\eta = \frac{m_1 m_2}{m^2}$, r is the radius, G is the gravitational constant, c is the speed of light, and m is total mass.

The first demonstrated evidence of a gravitational wave was not observed until the discovery of the Hulse-Taylor Binary by Hulse and Taylor [2]. PSR B1913+16 consist of a pulsar and an unseen neutron star companion as seen in Figure 21.2 [4]. This system represented proof of gravitational waves due to its steady decrease in orbital period which was able to be timed due to the pulsar. The systems expected time of periastron decreased by approximately 40 seconds over a 30 year span. This time loss from the expected showed a loss of energy in the system. The energy loss was then compared with the equation of energy loss for a gravitational wave [2].

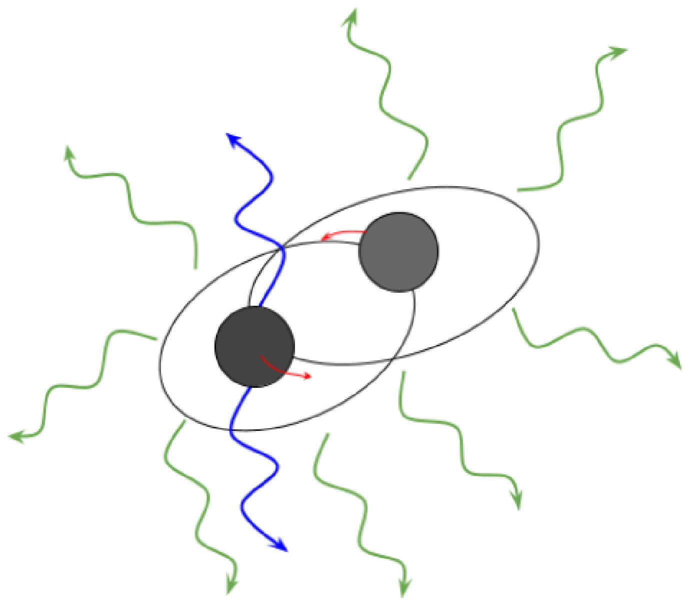

Figure 1.2: When a Pulsar and Neutron Star are in a binary system together they produce gravitational radiation in the form of gravitational waves (Green Arrows). These waves effect the period of the system which is easily measured due to the pulsar being emitted (Blue Arrows).

1.2 Sources of Gravitational Waves

Gravitational waves can come from a variety of sources including rapidly spinning neutron stars, supernovae, and stochastic sources from the early universe [4]. Gravitational waves from stochastic sources can be considered analagous to the cosmic microwave background. Each of these sources represent a potential path of research, but will not be the focus here.

A fourth source, and the focus of this paper is gravitational waves generated by compact binary coalescences (CBCs). This source can be split into three subcategories consisting of which compact objects make up the binary system. The first is two binary black holes (BBH) [2]. The second consists of two binary neutron stars (BNS). The third is a black hole and a neutron star (NSBH).

CBCs form gravitational waves as part of their orbital inspiral and eventual merger [2]. The gravitational waves generated by these events then find their way to Earth where they are detected. By knowing the parameters of the system we can predict the form of the wave generated. There are six parameters of the system to consider of which three are particularly important for detection [5]. The first of the system's parameters is the chirp mass *M*. The chirp mass of the system is equal to $(m_1 m_2)^{\frac{3}{5}}(m_1 + m_2)^{-\frac{1}{5}}$ where m_1 and m_2 are the components masses. The second parameter is the symmetric mass ratio η. The third parameter is ι, the inclination angle [5]. This is the angle between the orbital angular momentum vector of the system and the line of sight. The fourth parameter is the luminosity distance, d_L. Luminosity distance is defined by the relationship between absolute and apparent magnitude. The fifth parameter is an arbitrary reference time t_c. This time is normally set as the time of coalescence for the binary system. The sixth parameter of the system is ϕ_c. ϕ_c is defined as the waveform at t_c. These six parameters are used in conjunction with α, δ, and ψ which are right ascension and declination of the source, and polarization angle respectively to generate the waveform of a CBC [5].

While there are six parameters we can use to predict what a signal from a CBC will look like, and that we can find from a signal once we detect it, we first need to detect the signal. The signals of gravitational waves from CBC sources are chirping sinusoids without a known phase [6]. The signal normally enters the detectors observational band at around 10-20 Hz [5]. The signal is then processed and interpreted through a system called match filtering in which template banks of possible waveforms that a CBC signal could take are generated using component masses as the parameter. Any incoming signal is then compared to these templates to find a potential match [6].

As previously discussed the strain is the distortion of space as a gravitational wave passes through. This strain can be defined using the parameters of the waveform which takes the shape of a quadrupole [7]. With this there are two equations for strain, one in the plus and in the cross direction. The superposition of these equations is approximately equal to the strain detected by LIGO detectors.

$$h_+ = 2\frac{\boldsymbol{M}}{d_L}(1 + cos^2(i))(\pi \boldsymbol{M} f)^{\frac{2}{3}} cos(\Phi + \Psi) \tag{1.2}$$

$$h_x = 4\frac{\boldsymbol{M}}{d_L} cos(i))(\pi \boldsymbol{M} f)^{\frac{2}{3}} sin(\Phi + \Psi) \tag{1.3}$$

While Equations 1.2 and 1.3 work to understand the strain, LIGO currently uses a more advanced model that utilizes additionaly parameters.

1.3 Gravitational Wave Detection

LIGO and Virgo are two of the most well known gravitational wave detectors. Both of these groups use modified Michelson Interferometers to detect gravitational waves [8]. A Michelson Interferometers basic function is to use a beam splitter to split a laser down two arms. The beam is then reflected back and recombined into a single beam and passed into a detector as seen in Figure 1.3.

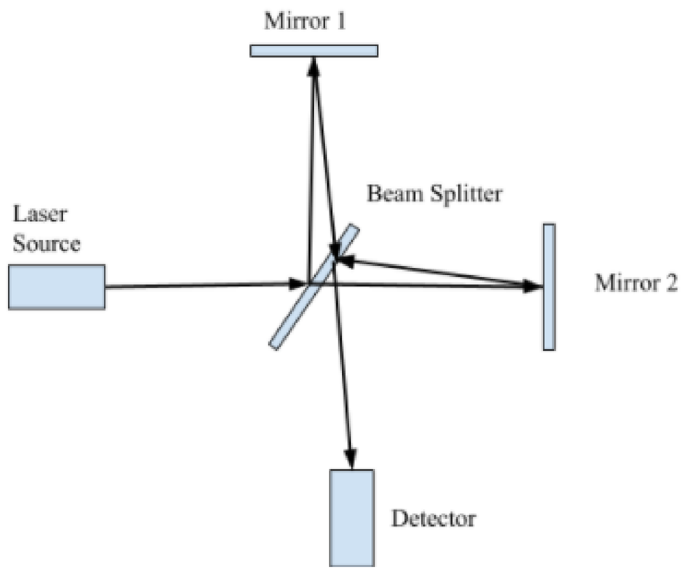

Figure 1.3: A simple Michelson Interferometer splits a beam with a beam splitter, has the beam go to the end of the arms, reflect back, and be recommbined before being passed to the detector. While this simple system is displayed in this figure, LIGO detectors add several other components to enhance the sensitivity and accuracy of the detecetor

The interferometers for the LIGO group have been modified from that basic concept to include a Fabry-Perot resonant chamber in both arms of the detector [8]. The detectors also include signal recycling to maintain a broad detector frequency response and detection band of 10 to 7000 Hz. The most sensitive portion of this band in the LIGO detectors is around 100 Hz. The laser used by LIGO is a multistage ND:YAG laser with a power of up to 180 W at the system output. Each arm of the LIGO detectors is 4km long [8].

The interferometer is able to detect a passing gravitational wave due to the effects of the wave on the arm length. While a wave is not passing through the mirrors in each arm are separated by L_x=L_y=L=4km, but during a gravitational wave these arms are distorted and are instead measured as ΔL(t) = $\delta L_x - \delta L_y$ = h(t)L where h is the gravitational wave strain amplitude [2]. This difference alters the beams phase as the two beams recombine after passing through the arms. The difference allows an optical signal to be transmitted to the detector that is proportional to that of the gravitational wave strain. These signals are often very small, so LIGOs detectors include an optical resonant cavity able to boost signals by a factor of 300 [2].

The first success of these detectors occurred on September 14th, 2015 when LIGO detected the first direct measurement of a gravitational wave at its two sites, Hanford, Washington and Livingston, Louisiana [9]. This detection was determined to be the merging of a $36M_\odot$ black hole and a $29M_\odot$ black hole into a $62M_\odot$ black hole releasing $3.0M_\odot$ worth of energy. This event occurred approximately 1.3×10^9 light years from Earth. This event occurred within the same month of the Advanced LIGO detectors coming online after receiving upgrades. Since this point many detections have been made including one on August 17th, 2017 when the first observation of an electromagnetic counterpart and afterglow were observed [1]. This detection was the beginning of multi-messenger astronomy.

LIGO and Virgo, another detector located in Italy, will soon be joined by two more ground based detectors. The Kamioka Gravitational Wave detector (KAGRA) in Japan will add to the existing detectors allowing for more accurate detection of gravitational waves and their location [10]. Additionally, LIGO-India will be built at some time in the future to further bolster the ground based detector network [11].

LIGO and Virgo are not alone in detecting gravitational waves. The International Pulsar Timing Array (IPTA) uses pulsar timing arrays to detect gravitational waves through the monitoring of pulsar rotational periods [12]. Additionally, the Laser Interferometer Space Antenna (LISA) will largely expand the signals at which gravitational waves can be detected [13]. In particular LISA will allow for the detection of gravitational waves between 0.1 and 100 mHz, a frequency range currently outside the range of ground based detectors.

Chapter 2

Multi-Messenger Astronomy

2.1 What is a Multi-Messenger Astronomy?

Throughout the history of astronomy, observations have been stuck in the electromagnetic spectrum. Humans were able to observe light in various waelengths, but that was the extent of our abilities. Multi-messenger astronomy opens a door beyond the electromagnetic spectrum. Things like gravitional waves and particles such as the neutrino are now detectable allowing for areas of the universe that were previously unobservable to now be opened up to mankind [14].

Multi-messenger astronomy is progressing with multiple different messengers seeing advancements. As seen in Table 2.1, the various sources range in energy and frequency. Gravitational waves are one of the predominant aspects of multi-messenger astronomy as they offer a medium of observation distinctly different than the electromagnetic spectrum. As previously discussed the sources of gravitational waves vary, but those applicable to multi-messenger astronomy can be grouped into three general categories [14]. Persistent sources of gravitational waves include pulsars paired with a neutron star or binary neutron stars and binary white dwarfs are one category. A second category includes bursting sources from core collapse events such as supernovae. The category this thesis will focus on is inspiral sources such as BBH, BNS, and NSBH merger events. Outside of gravitational waves, neutrinos also offer a gateway into multi-messenger astronomy. Neutrinos have not yet seen the success of gravitional waves in finding a counter part in another messenger medium, but events such as gamma-ray burst offer potential for such a ground breaking detection [14]. A third messenger that may help in multi-messenger astronomy is ultra-high-energy cosmic rays. This messenger is closely tied to astrophysical neutrinos, however the rays are made of relativistic, massive charged particles that do not reach the speed of light. These particles do present a challenge as they are affected by magnetic fields leading to deviation in their direction and travel time. This makes these rays hard to trace back to a particular source [14].

Multi-Messenger Sources	
Electromagnetic Spectrum	
Name	Wavelength
Radio	1mm - 100km
Microwave	1mm - 100mm
Infrared*	750nm - 1mm
Visible*	380nm - 760nm
Ultraviolet*	10nm - 400nm
X-ray	10pm - 10nm
Gamma ray	$<$ 100pm
Neutrinos	
Solar Neutrino	Lower Energy
High Energy Neutrino	Higher Energy
Gravitational Waves	
Source	Frequency
Persistent Sources	0.1mHz [15]
Inspiral Sources	10Hz - 7000Hz [8]
Core-collapse Events	UNKNOWN

Table 2.1: The sources of multi-messenger astronomy and their related measurements [14]. *Wavelengths in the near infrared and ultraviolet along with the visible spectrum make up the opitcal spectrum used by optical astronomers.

While multi-messenger astronomy has recently seen major advancements, the era of transient multi-messenger astronomy began around 30 years ago with the detection of SN1987A [16]. SN1987A was a core-collapse supernova in the Large Magellanic Cloud (LMC). Due to the LMC's popularity in astronmical studies, the supernova was detected early on through random chance. In an independent search a burst of MeV neutrinos were detected only hours before hand. These two events were clearly linked and led to further studies into the event. This first instance of multi-messenger astronomy led to confirmations of supernovae produced in the formation of Neutron Stars and Black Holes, along with revealing a host of new science.

The IceCube group has also established a foot hold in multi-messenger astronomy [16]. IceCube observes neutrinos that track to the X-ray emmission. By providing real-time alerts, IceCube enables the Swift satellite to perform rapid follow up of potential astrophysical neutrino events. This follow up led to the detection of the blazar TXS0506+056. TXS0506+056 was the brightest GeV flare observed in the past decade of observations. This observation led to an extensive follow up effort. This follow-up is credited with the first detection of a source at very high energies. TXS0506+056 is another example of multi-messenger astronomy resulting in the discovery of new science.

The world of multi-messenger astronomy saw another large leap forward on August 17th, 2017 when a BNS coalescence, GW170817, was detected [1]. This gravitional wave detection was the first to be followed up by the observation of an electromagnetic counterpart as well as afterglow in the gamma-ray, UV, optical, infra-red, and radio spectrums. The detection gave rise to several scientific findings, but it also showed that the detection of an event with multiple mediums of detection was possible. GW170817 helped provided a new way to measure cosmological parameters such as the Hubble constant, confirmed that mergers produce heavy elements in their aftermath, set a limit on the speed difference of gravitational waves and light, and helped answer questions about the origin of short gamma-ray burst. All of these findings came from a single multi-messenger event. As more occur, more answers may arise.

An important thing to note about GW170817 is the response time from merger event to follow up observations. The gamma-ray burst was detected approximately 2 seconds post merger event, but the remaining observations did not occur until approximately 8 hours after the merger [1]. This time delay was in part due to a glitch at the Livingston interferometer and data transfer issues from the Virgo detector to analysis sites, which led to the alert going out apprximately 40 minutes after the event and sky localization going out 4.5 hours after the signal was detected. The glitch and data transfer issue aside, the time to send out warnings and attempt to follow up on events is a focus of this paper. As early warning of inspiral events improves, the warning time given to other observers will increase. Currently BNS sources with low enough redshift can be detected approximately 10 - 60s before the merger. From the BNS mergers detected before merger approximately 2% can be detected within 100 deg^2 with a 90% credible interval [1].

2.2 The Future of Multi-Messenger Astronomy

Multi-messenger astronomy is rapidly becoming a crucial part of the broader astronomical scientific community. Work to improve and refine methods of multi-messenger astronomy continue to push forward the accuracy and ease of combining multiple sources such as gravitational waves and their electromagnetic counterparts. These attempts show a peak into what the future of multi-messenger astronomy will be. One of the most important aspects of this peak into the future is early warning systems. These systems allow for electromagnetic follow-up to be possible rather than relying on coincendatal observations or post-merger observations alone.

When looking towards the future of multi-messenger astronomy and the early warning system for gravitational waves it is important to look at the work done previously. This paper will be building off of the previous work done by Sachdev et al. [1]. That paper looked at the pre-merger detection of BNS coalescences at frequencies starting at 10 Hz and going to 29 Hz, 32 Hz, 38 Hz, 49 Hz, 56 Hz, and 1024 Hz. Each of these frequencies, refered to as runs, approximate to a signal recovery time of 58 s, 44 s, 28 s, 14 s, 10 s, and 0 s before merger respectively. The exact methods utilized will be discussed later in Chapter 3, but to simplify the process, simulated BNS signals were generated. These signals, refered to as injections, are inserted uniformly into Gaussian data. There is then an attempt to recover the signals using matched-filtering (see Section. 3.1). For each run a false alarm rate (FAR) $<=$ 1/(30 days) for an injection is considered found in each of the 6 runs. The paper computed the expected number of signals for each run using the sensitive spacetime volume based on the FAR threshold and local BNS merger rate. This is then estimated to

$$\langle VT \rangle = \langle VT \rangle_{injected} \frac{N_{recovered}}{N_{totalsims}} \tag{2.1}$$

where $\langle VT \rangle$ is sensitive spacetime volume, $N_{recovered}$ is the number of recovered injections at the given FAR, and $N_{totalsims}$ is the total number of simulated signals. $VT_{injected} = 0.178 Gpc^3 a$ for the signal distribution used in this paper. The results can be seen in Table 2.2 [1].

f_{high}(Hz)	$\langle VT\rangle(Gpc^3a)$	$N_{signals}(a^{-1})$	$N_{low} - N_{high}(a^{-1})$
29	$2.55x10^{-4}$	3.21	$0.775 - 8.71$
32	$3.84x10^{-4}$	4.84	$1.17 - 13.2$
38	$7.23x10^{-4}$	9.12	$2.20 - 24.8$
49	$1.45x10^{-3}$	18.2	$4.41 - 49.5$
56	$1.88x10^{-3}$	23.6	$5.71 - 64.2$
1024	$3.86x10^{-3}$	48.7	$11.8 - 132$

Table 2.2: The senstive spactime volume, $\langle VT\rangle$, and the expected number of signals, $N_{signals}$, per year based on median BNS merger rate as presented in Sachdev et al. [1]

The early detection of mergers is important, but detecting the mergers is not enough. In order for multi-messenger astronomy to progress, pre-merger detections need to aid electromagnetic observations. To do this sky localizations are neccessary. LIGO-Virgo use BAYESTAR to generate rapid localizations [1]. BAYESTAR is a fast Bayesian algorithm able to reconstruct GW transients positions using the output of a matched-filtering search. In the Sachdev et al paper, passing the signal to noise ratio (SNR) time series of all the injections passing the FAR threshold to BAYESTAR resulted in Figure 2.1. The figure shows the cumulative distribution of the sky localizations at a 90% credible interval. The right axis of the number of events expected each year as a function of the largest localization area given the median merger rate. The left axis shows the right axis value as a fraction of the total injections recovered at full bandwidth.

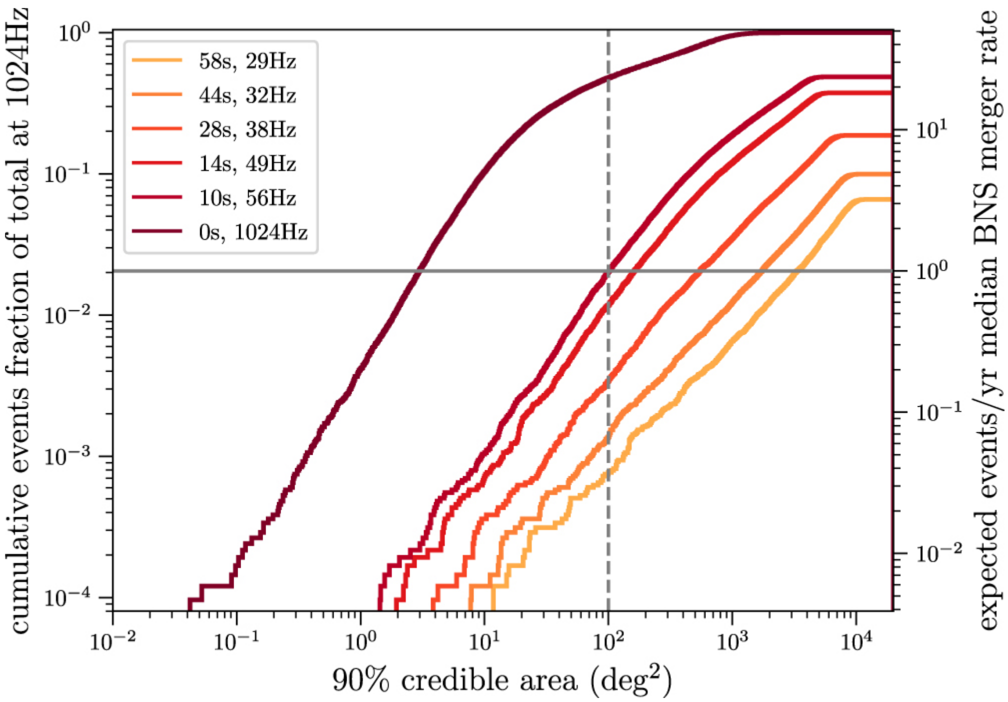

Figure 2.1: The figure shows the cumulative distribution of the sky localizations at a 90% credible interval. The right axis of the number of events expected each year as a function of the largest localization area given the median merger rate. The left axis shows the right axis value as a fraction of the total injections recovered at full bandwidth. [1].

The goal of sky localization is to provide a small search area. This is important due to the small field of view that optical telescopes have. In Figure 2.1, we see that there is at least one event per year that is both detected pre-merger and localized within $100deg^2$ [1]. By considering the area of the sky searched according to the localization PDF before finding the true location, the number of events detected before merger and before searching over $100deg^2$ becomes about 9 events per year. The search area can be further reduced using imagining strategies informed by galaxy catalogs. Early warning events, particularly those that arre well localized, the source of the events are typically closer than sources that are not detected in early warning. A minimum of 1 event per year that is detected 60s before merger will be within 100Mpc and 13 events per year will be within 200Mpc and be detected pre-merger. In Sachdev et al. data transfer, calibration, and matched-filterng processes are assumed to produce no latency. They state that the actual latency is approximately 20s with a goal of reducing that time to approximately 7s for smaller bandwidth configurations.

Optical telescopes such as the BlackGEM array, Zwicky Transient Facility, the Dark Energy Camera, the Rubin Observatory, the Swope Telescope, and the Subaru Telescope along with other similar wide-field optical transient facilities are the best suited to optical follow-up for well localized events [1]. The Fermi Gamma-ray Burst Monitor and the Swift Observatory offer a follow-up option for events with larger localization areas. The early warning alerts of pre-merger GW are particularly helpful in identifying threshold gamma ray bursts. Large FOV radio telescopes such as the Murchison Widefield Array, the National Radio Astronomy Observatory, the Giant Metre-Wave Radio Telescope, the Owens Valley Long Wave-length Array, the Square Kilometre Array, and other similar radio telescopes are useful in early warning alerts that are poorly localized as well as those with good localization. Gamma-ray follow up of alerts can be done by detectors such as the Cherenkov Telescope Array. This follow up heavily relies on the early warning alert as it must be pointed at the source at the time of merger as there is no detectable hypothesized afterglow.

Chapter 3

Methods

3.1 Matched Filtering

The primary method of detecting gravitational waves in the signals collected by the LIGO detectors is called Matched Filtering. Matched filtering is a useful technique when the form of the signal is known accurately [17]. Unfortunately, while we know the form of the signal we do not know all the parameters. In order to find the parameters of the signal we attempt to match the raw signal to a waveform with known parameters called a template or filter. The fourier transform of the template is equal to the fourier transform of the signal divided by the noise power spectrum. By looking at the maximum correlation with the templates it can be determined whether or not an event signal is present.

In situations where the parameters of the template match those of the signal we get a boost to the SNR [17]. This boost is proportional to the square root of the number of cycles the signal spent in the detector output. When the waveform's shape is unknown the signal is filtered to the frequency band where the signal is assumed to lie. At this point the signal to noise ratio is looked at for each time domain indiviudally. Additionally, for the matched filtering process to be fully successful, the inspiralling binary waveform must be known accurately. The most important aspect of the waveform that needs to be considered is the evolution of the waveform's phase. If the phase is mismatched between the signal and template the SNR is significantly reduced.

To detect the signal parameters, the signal must be passed through a number of templates [17]. The number of templates required depends on the number of parameters the signal has. A gravitional waveform can be defined by four parameters. The first two parameters are dependent on the starting conditions. These are t_a, the time of arrival and Φ, the phase at arrival. The second two are both the chirp mass. The first chirp time is the Newtonian chirp time, while the second considers past-Newtonian corrections to the chirp time. The number of parameters increases the amount of templates needed to determine the parameters so any reduction in the number of parameters is seen as a benefit. Because of this, it was found that both the Newtonian and post-Newtonian chirp time closely correlate to each other and can be reduced to a single parameter. This reduction leaves the signal with only three parameters to find using the templates. The correlation between the chirp times only holds while near the maximum of the correlation function, meaning the reduction to three parameters only holds for certain circumstances.

In the case of LIGO-Virgo data, we use the GstLAL-based inspiral pipeline, a low-latency mathced-filtering pipeline designed for the detection of gravitational waves from compact binary coalescences [1]. GstLAL groups templates into smaller sub-banks based on intrinsic parameters of the template that impact their response to noise. From this it uses the LLOID method, which performs multi-banding and singular value decomposition of individual time slices to build orthogonal basis filters from the sub-banks. By cross-correlating the incoming data with the basis filters, GW wave canidiates can be found.

In order to reduce the number of event candidates to be looked at any canidate with an SNR of less than 4.0 is discarded [1]. Following this canidates are ordered by their SNR, detector sensisitivty at the time of event trigger, a signal consistency test, and the time and phase delays between detectors. This is done by finding the log-likelihood ratio for each canidate. The next step is to create the distribution of log-likelihood ratio for noise triggers. To do each parameter of the log-likelihood ratio has its noise distribution sampled. From there a false-alarm-rate (FAR) is assigned to each canidate. The false-alarm-rate describes how often noise will create a canidate of the given appearance without an actual event occuring.

3.2 Real Time Anlaysis

The LIGO collaboration's work to detect gravitaional waves involves a large amount of data collection. During operation, the laser interferometers collect a near continuous stream of data, meaning the detection of events occurs simultaneously with other data collection. Because of this, a variety of tools have been developed to aid in the viewing of incoming data with minimal delay. These tools take in the signals from the detectors after they have traveled through the processing pipeline and display them in plots of SNR, FAR, IFAR, and other useful plots of the incoming data as is displayed in Figure 3.1. These plots all cover a set amount of time which automatically updates as more data enters the dashboard. Therefore you are always looking at the most up to date information. The dashboard does contain a way to manually set the time range you are looking at in order to go back to certain events that have occured. In this way you can look at events as they first show up on the dashboard.

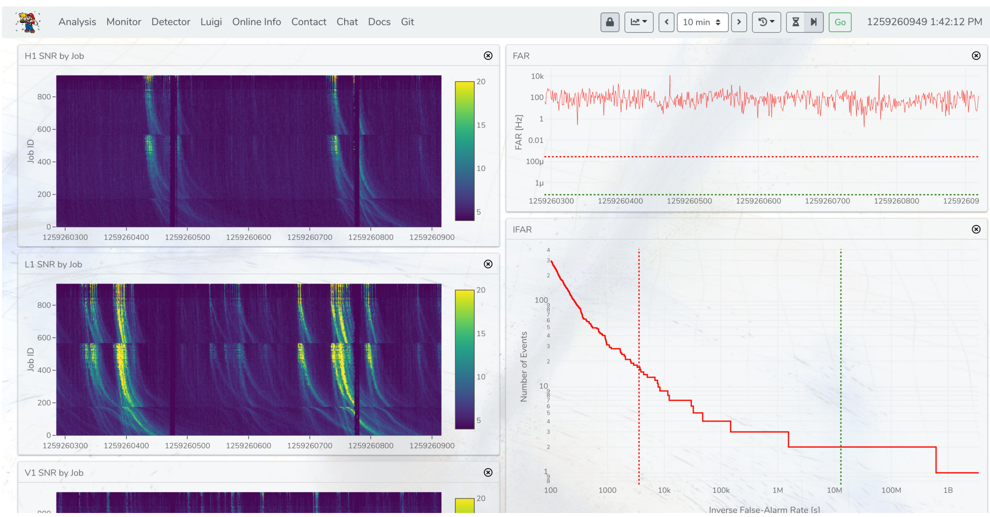

Figure 3.1: The SCALD dashboard shows a variety of useful plots including SNR by Job for each detector, the FAR over time, and the inverse FAR

These plots all represent important information in the detection of gravitational wave events. The SNR shows when a gravitational wave has been detected as an event will have cause a spike in SNR. By checking the FAR, it can be ensured that any event detected is an actual event and not the result of random noise. The IFAR visually shows the amount of time expected before a false alarm event occurs, as it is the invese of the FAR. By displaying all of this information in real time, events flagged by the detection pipeline can be manually checked by observers.

3.3 Early Warning Capabilities

Early warning attempts to detect events pre-merger in a way that the initial detection pipeline does not. This is possible through the use of the low-latency matched filtering in the GstLAL-based inspiral pipeline. Early warning is possible when a large enough SNR accumulates before the merger occurs [1]. Events that accumulate enough SNR and pass a given FAR threshold are identified within approxiately 1 minute of the gravitaional-wave signals reaching the Earth [18]. Although detection times can be as fast as 1 minute after the signal reaches Earth the distribution of an alert does not occur at that same rate due to the presence of latencies [1]. Data transfer, calibration, filtering, and other follow-up processes result in latencies of approximately 20 s. It is predicted that these times will be reduced to approximately 7 s for future early warning alerts.

3.4 Generation of Simulated Data

In order to test the early warning process, we simulate data that mimics the actual signals that LIGO detects. In order to make the signals realistic, event signals are intermixed with noise. An early paper by Sachdev et al. accomplished this using Gaussian data to simulate noise [1] This Gaussian data is recolored to fit with the Advanced LIGO and Advanced Virgo design sensitivities. In that study they generated 1 month of stationary data. This was then combined with 1918947 simulated BNS signals. These signals are referred to as injections and are simulated with components masses of $m_1 < 1.0 M_\odot$ and $m_2 < 2.0 M_\odot$. The model simulates a population of neutron stars that are non-spinning. They are distributed uniformily with a redshift up to $z = 0.2$. The Sachdev et al. rejected 1659747 of the injections made as their SNRs fell below 3. The remaining injections were inserted into the Gaussian noise.

One key difference between the study carried out by Sachdev et al. and the simulation done for this paper, is the nature of the noise. In the original study the noise is simulated using Gaussian Noise, where as in this paper we will be using noise that more closely mirrors that of LIGO data. This updated method of noise simulation will include glitches in the signal that effect the detection of injections, meaning that it will more accurately predict the effectiveness of the early warning detection.

3.5 Simulating Early Warning Searches

The simulation of the live early warning search utilizes matched filtering, just as it would in the live detection pipeline. The matched-filtering done in both the previous study by Sachdev et al. and here uses a template bank composed of GW waveforms that fall within the parameter space we are looking at [1]. In particular, templates for both studies were made assuming components masses of $m_1 < 0.95 M_\odot$ and $m_2 < 2.4 M_\odot$. The bounds chosen also account for redshift and edge effects, and expect a chirp mass between $0.9 M_\odot$ and $1.7 M_\odot$.

In the original paper, Sachdev et al. repeated their search 6 times using the same template bank and dataset to look at various end frequencies [1]. These frequencies correspond to different times before merger and are only approximate due to grouping of waveforms such that they have the same pre-merger time. In particular, 29 Hz, 32 Hz, 38 Hz, 49 Hz, 56 Hz, and 1024 Hz, were looked at. These correspond to approximately 58 s, 44 s, 28 s, 14 s, 10 s, and 0 s before the merger occurs. In this paper we will look specifically at 49 Hz or 14 s before merger using the conditions described in Table 3.1.

Settings	
Start Time	1238166018
End Time	1240757018
Frequency	49Hz
Low Frequency Cutoff	10.0
High Frequency Cutoff	49
Sample Rate	2048
Number of Split Templates	500

Table 3.1: List of settings used to generate the analysis of the simulated data

In order for an injection to be considered found, it must meet a certain FAR threshold. For Sachdev et al. this threshold had to be met in all 6 different frequency runs, but for us only the 49 Hz frequency will be considered. For both the original study and our own the FAR threshold was set to FAR <= 1/(30 days) [1]. Once an injection is considered found, sky localization can be done. This step is accomplished by generating the SNR time series of all found injections and providing those time series to the BAYESTAR tool to localize the signals.

Chapter 4

Results

4.1 Effectiveness of Early Warning

The results of this study can be seen visually in the form of a variety of plots. These results highlight the current state of early warning by simulating realistic noise. We can further establish where early warning stands by comparing our results with simulated data using Gaussian noise. Overall the results show there is marked room for improvement in the early warning pipeline.

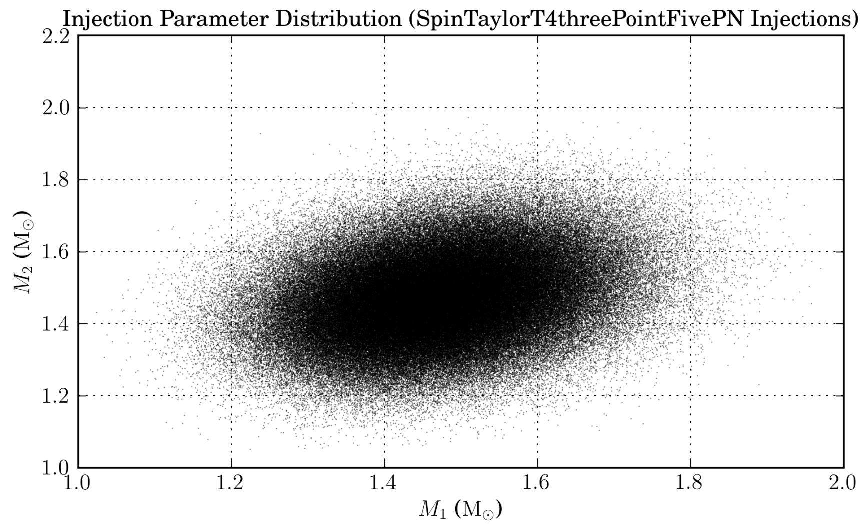

Figure 4.1: This plot shows the component masses of the generated injections.

Within Figure 4.1 we can see the distribution of injected parameters. The majority of parameters' component masses fall approximately between $1.2M_\odot < M_1 < 1.8M_\odot$ and $1.2M_\odot < M_2 < 1.8M_\odot$. These injections were the target of detection in this study.

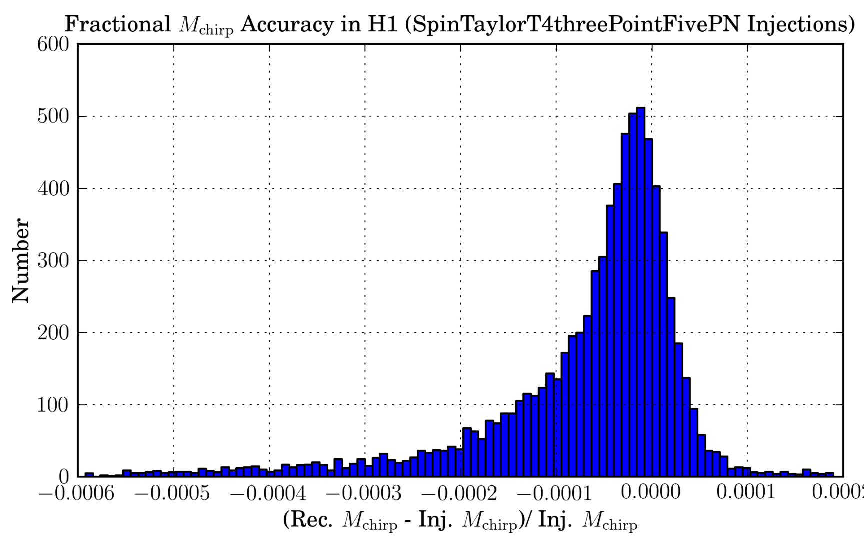

Figure 4.2: This plot shows the accuracy of the detected chirp masses. While there is a slight tail towards recovered injections having smaller chirp masses than expected, the majority of chirp masses recovered are within close proximity to the injected chirp mass.

In Figure 4.2, the fractional accuracy of our recovered chirp mass is plotted. As is seen the peak lies only slightly off of the 0 line, meaning that our recovered chirp masses are very close to those injected for the majority of injections. While this plot only covers the Hanford detector similar results were seen in the Livingston and Virgo recovered chirp masses.

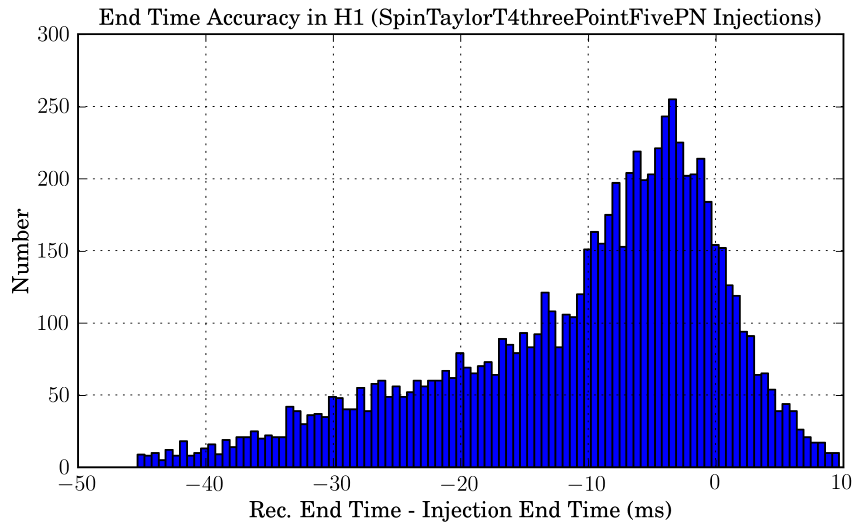

Figure 4.3: This plot shows the difference in recovered signal end time and the injection end time in the Hanford detections. This demonstrates the accuracy to which we can determine the merger time before the merger event.

Figure 4.3 shows the accuracy of the recovered end times. The plot shows that with significant accuracy a signals end time can be detected within 5 ms of the actual injection end time. While this plot is only of the Hanford detector, similar results were found for both the Livingston and Virgo detectors.

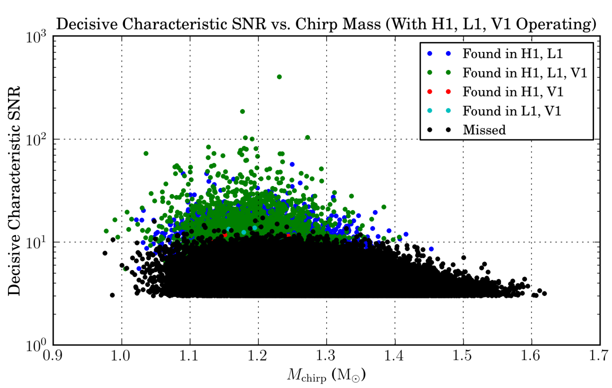

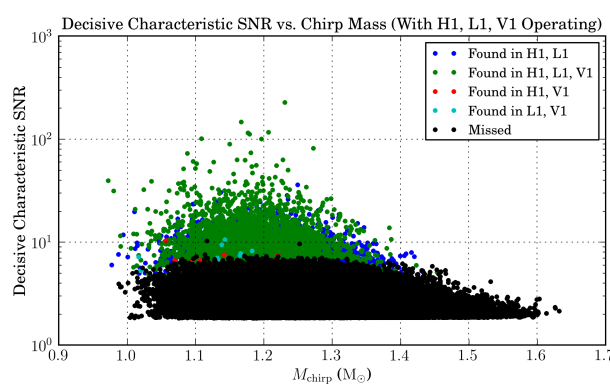

Figure 4.4: The left figure shows the SNR vs Chirp Mass of the injections put into the simulated "Real" Noise. The points are labeled with which detectors found the injection. The right figure shows the SNR vs Chirp Mass of the injections put into the simulated Gaussian Noise as discussed in Sachdev et al. [1]. The points are labeled with which detectors found the injection.

Figure 4.4 shows which injections are detected in the early warning with Gaussian noise and with "Real" noise. In the left panel, injections with SNRs at and below 10 are not detected. This is in contrast to the right panel, where injections below 6 are predominantly not detected. With an SNR of 10 being the limit for the "Real" Noise, it is evident that the early warning process needs more refinement. Ideally, we would match the Gaussian Noise SNR limit as a sign that the early warning detection methods are improving.

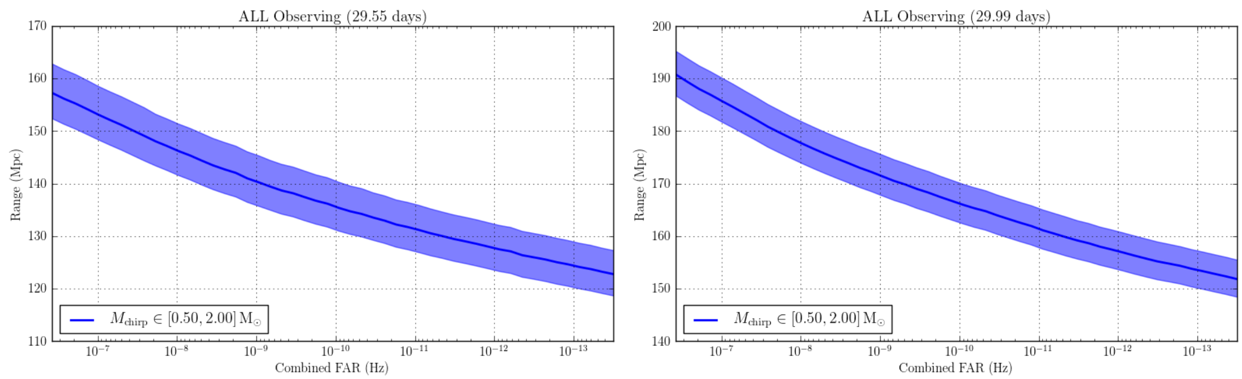

Figure 4.5: The left figure shows the range that a chirp mass can be detected at with a given FAR with injections embedded in simulated "Real" Noise. The left figure shows the range that a chirp mass can be detected at with a given FAR with injections embedded in Gaussian Noise as done in Sachdev et al. [1]. In both plots a FAR of 10^{-7} represents approximately 1 detection a month.

Figure 4.5 both show the range at which a chirp mass can be detected with a given FAR. The higher this range the better as it indicates higher detection sensitivity. As is clear from the plots, when using the "Real" Noise simulation the range is significantly dropped representing approximately 1.84 times fewer event detections. This drop suggest that the early warning method still needs improvements to increase its sensitivity to be on par with that of the Gaussian noise simulation. As it currently, functions the "Real" Noise simulation cannot accurately detect as many mergers. This reduction limits indicates a need to improve the early warning method.

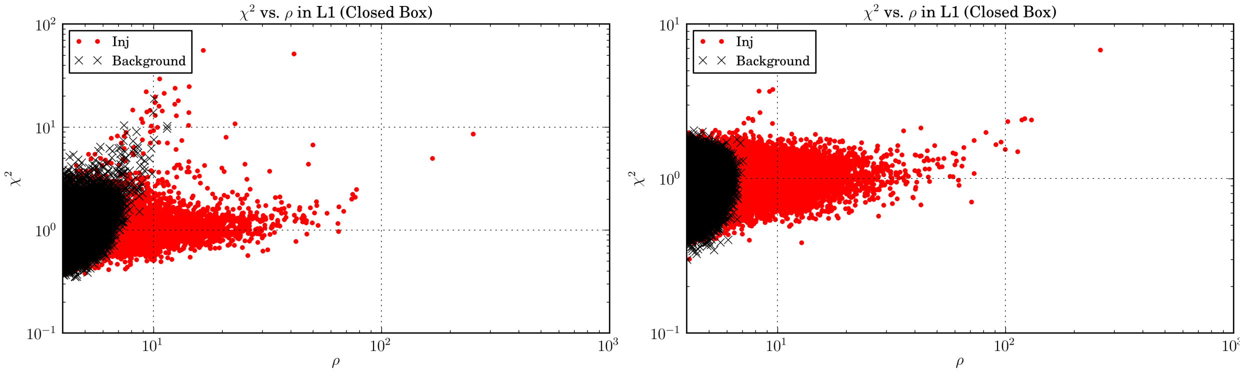

Figure 4.6: The left figure checks that the SNR accumulated matches the expectations for injections made into simulated "Real" Noise. The right figure checks that the SNR accumulated matches the expectation for injections made into Gaussian Noise [1].

Figure 4.6 shows the χ^2 plotted against ρ. The χ^2 allows us to check that the SNR accumulated is the same as expectations. Both plots have similar shapes, but the background and injections in the plot generated with "Real" Noise includes an offshoot going upwards past 10 that is not present in the plot made for Sachdev et al.

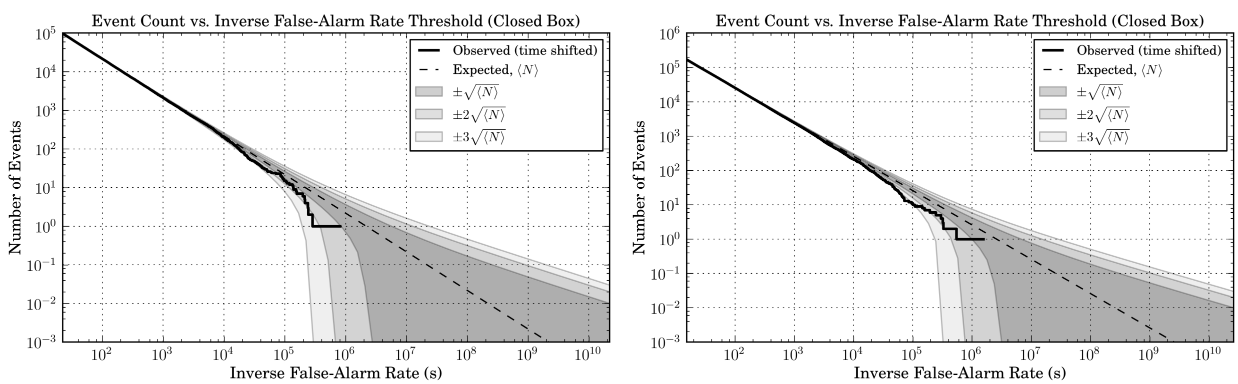

Figure 4.7: The left plot, often referred to as the Money Plot, shows the number of events vs the inverse FAR when injections are made into simulated "Real" Noise. The right plot shows the same information when injections are made into Gaussian Noise as done by Sachdev et al [1]. Both tells us that the FAR is valid despite their respective noise.

Figure 4.7 shows very similar plots from both the "Real" Noise and Gaussian Noise studies. This similarity is good as it shows that the "Real" Noise test of early warning did work as the FAR is still valid regardless of the noise. While the other plots show us some shortcomings in early warning, this plot does imply that the method is working.

Chapter 5

Conclusion

5.1 Summary

This study sought to test the early warning system using a simulation that more closely mirrored live LIGO detection. This was done by simulating "Real" Noise and injecting signals into this noise in order to test the early warning system. These tests were compared to the previous work done by Sachdev et al. which carried out a similar assessment of the early warning system, but using Gaussian Noise. These comparisons showed that the early warning system still has room to improve as it missed injections with SNRs from 10 to 6 that were previously found in Sachdev et al. Additionally, the range at which the early warning method was sensitive was decreased in this study when compared to that of Sachdev et al. While these areas showed weaknesses, the study did have a Money plot that was similar to that of Sachdev et al. demonstrating that, while the "Real" Noise did decrease the effectiveness of the early warning method, it did still work as expected.

5.2 Future Work

This experiment focused solely on testing early warning at 49 Hz. Sachdev et al. tested a wider range of frequencies that correlated to an early warning time of up to 1 minute. Future studies can repeat the work done in this paper for the remaining 5 frequencies; 29 Hz, 32 Hz, 38 Hz, 56 Hz, and 1024 Hz. Additionally, further work can be done to increase the warning time that the early warning method provides. This can be done by reducing latency at various stages of the proccess including signal processing such as matched filtering. Other work can be done to increase the accuracy of the early warning method. While the goal of early warning is to make fast detections, these detections also need to be correct, as other astronomers rely on these signals to carry out follow up observations. Between the other frequencies, increased speed, and increased accuracy early warning still has plenty of room to improve.

Bibliography

[1] S. Sachdev, R. Magee, C. Hanna, K. Cannon, L. Singer, D. Mukherjee, S. Caudill, C. Chan, J. D. Creighton, B. Ewing, *et al.*, “An early-warning system for electromagnetic follow-up of gravitational-wave events,” *The Astrophysical Journal Letters*, vol. 905, no. 2, p. L25, 2020.

[2] B. P. Abbott, R. Abbott, T. Abbott, M. Abernathy, F. Acernese, K. Ackley, C. Adams, T. Adams, P. Addesso, R. Adhikari, *et al.*, “Observation of gravitational waves from a binary black hole merger,” *Physical review letters*, vol. 116, no. 6, p. 061102, 2016.

[3] C. J. Moore, R. H. Cole, and C. P. Berry, “Gravitational-wave sensitivity curves,” *Classical and Quantum Gravity*, vol. 32, no. 1, p. 015014, 2014.

[4] K. Riles, “Gravitational waves: Sources, detectors and searches,” *Progress in Particle and Nuclear Physics*, vol. 68, pp. 1–54, 2013.

[5] J. Aasi, J. Abadie, B. Abbott, R. Abbott, T. Abbott, M. Abernathy, T. Accadia, F. Acernese, C. Adams, T. Adams, *et al.*, “Parameter estimation for compact binary coalescence signals with the first generation gravitational-wave detector network,” *Physical Review D*, vol. 88, no. 6, p. 062001, 2013.

[6] K. Cannon, A. Chapman, C. Hanna, D. Keppel, A. C. Searle, and A. J. Weinstein, “Singular value decomposition applied to compact binary coalescence gravitational-wave signals,” *Physical Review D*, vol. 82, no. 4, p. 044025, 2010.

[7] L. S. Finn and D. F. Chernoff, “Observing binary inspiral in gravitational radiation: One interferometer,” *Physical Review D*, vol. 47, no. 6, p. 2198, 1993.

[8] J. Aasi, B. Abbott, R. Abbott, T. Abbott, M. Abernathy, K. Ackley, C. Adams, T. Adams, P. Addesso, R. Adhikari, *et al.*, “Advanced ligo,” *Classical and quantum gravity*, vol. 32, no. 7, p. 074001, 2015.

[9] B. P. Abbott, R. Abbott, T. Abbott, M. Abernathy, F. Acernese, K. Ackley, C. Adams, T. Adams, P. Addesso, R. Adhikari, *et al.*, “Gw150914: The advanced ligo detectors in the era of first discoveries,” *Physical review letters*, vol. 116, no. 13, p. 131103, 2016.

[10] T. Akutsu, M. Ando, K. Arai, Y. Arai, S. Araki, A. Araya, N. Aritomi, H. Asada, Y. Aso, S. Atsuta, *et al.*, “Kagra: 2.5 generation interferometric gravitational wave detector,” *arXiv preprint arXiv:1811.08079*, 2018.

[11] L. S. Collaboration *et al.*, "Gravitational wave astronomy with ligo and similar detectors in the next decade," *arXiv preprint arXiv:1904.03187*, 2019.

[12] J. Verbiest, L. Lentati, G. Hobbs, R. van Haasteren, P. B. Demorest, G. Janssen, J.-B. Wang, G. Desvignes, R. Caballero, M. Keith, *et al.*, "The international pulsar timing array: first data release," *Monthly Notices of the Royal Astronomical Society*, vol. 458, no. 2, pp. 1267–1288, 2016.

[13] J. Baker, S. F. Barke, P. L. Bender, E. Berti, R. Caldwell, J. W. Conklin, N. Cornish, E. C. Ferrara, K. Holley-Bockelmann, B. Kamai, *et al.*, "Space based gravitational wave astronomy beyond lisa," *arXiv preprint arXiv:1907.11305*, 2019.

[14] A. Levan, "Multimessenger astronomy," in *Gamma-Ray Bursts*, 2514-3433, pp. 9–1 to 9–34, IOP Publishing, 2018.

[15] G. Nelemans, "The galactic gravitational wave foreground," *Classical and Quantum Gravity*, vol. 26, no. 9, p. 094030, 2009.

[16] E. Burns, A. Tohuvavohu, J. Bellovary, E. Blaufuss, T. Brandt, S. Buson, R. Caputo, S. Cenko, N. Christensen, J. Conklin, *et al.*, "Opportunities for multimessenger astronomy in the 2020s," *arXiv preprint arXiv:1903.04461*, 2019.

[17] B. S. Sathyaprakash, "Filtering post-newtonian gravitational waves from coalescing binaries," *Physical Review D*, vol. 50, no. 12, p. R7111, 1994.

[18] C. Messick, K. Blackburn, P. Brady, P. Brockill, K. Cannon, R. Cariou, S. Caudill, S. J. Chamberlin, J. D. Creighton, R. Everett, *et al.*, "Analysis framework for the prompt discovery of compact binary mergers in gravitational-wave data," *Physical Review D*, vol. 95, no. 4, p. 042001, 2017.

Academic Vita
Collin Heckman

Education

- ***Pennsylvania State University*** *2017-anticipated Spring 2021*
  - B.S. Astronomy and Astrophysics; B.S. Physics
  - Relevant Coursework:
    - ASTRO 414: Stellar Structure and Evolution
    - ASTRO 497: Introduction to Astrostatistics
    - PHYS 419: Theoretical Mechanics
    - PHYS 410: Intro Quantum Mechanics I
    - PHYS 400: Intermediate Electricity and Magnetism
  - **Schreyer Honors College** - Designed to promote academic excellence, leadership, and civic engagement while challenging students to gain a global perspective.

Research Experience

- ***Pennsylvania State University, Department of Physics*** *May 2019 - Present*
  - Working with a team of graduate students, post doctorates, and a leading faculty member in the Penn State LIGO group to develop tools using Python and HTML to efficiently detect gravitational waves from binary neutron star mergers, enabling other teams to observe the collision through various mediums

Awards and Scholarships

- **Millennium Scholars Program** - Merit-based full scholarship program designed to prepare future science leaders while supporting the pursuit of doctoral studies in science, technology, engineering and mathematics (STEM) disciplines.
- Braddock Scholarship
- Ira M. Lubert Scholarship
- President's Freshman Award and Dean's List
- Elsbach Honors Scholarship
- M & J Underwood Scholarship

Skills

- Computer programming (Java, Python, JavaScript, HTML, CSS)
- Verbal and written communicational
- Leadership/collaborative interpersonal skills
- Languages: English, first language; German, intermediate proficiency

Research Interests

- Gravitational Wave Detection and Instrumentation
- Binary Neutron Stars
  - Gamma-ray burst
  - Gravitational Waves from Neutron Star Mergers

Organizations and Activities

Boy Scouts of America *2007 - Present*

- Awards and Honors
  - James E. West Fellowship Award (2019)
  - Order of the Arrow Founders Award (2018)
  - Order of the Arrow Vigil Honor (2016)
  - Eagle Scout (2015)

- Leadership
  - Section Chief: Section NE-6B (Central Pennsylvania and parts of Maryland) (2018-2019)

    - Section Vice-Chief: Section NE-6B (2017-2018), Order of the Arrow Lodge Chief #39 (2016-2017)
    - National Leadership Seminar Trainer (Northeast Region)

Astronomy Club

- Co-President (2018-2019), Telescope Trainer -- Provide educational assistance to college and local community members during university and community events

Society of Physics Students

- Member supporting the learning and interest of physics within the college and local community

Science Lion Pride

- Recruitment Director -- Organize and plan tours and events for perspective science students
- Treasurer – Organize funds and merchandise for club members
- Participate and represent Eberly College of Science at alumni and community service events